JOURNAL OF MECHANICAL ENGINEERING AND SCIENCES
ISSN: 2289-4659 e-ISSN: 2231-8380
VOLUME 17, ISSUE 4, 2023, 9700 – 9714
DOI: https://doi.org/10.15282/jmes.17.4.2023.4.0768

UNIVERSITI MALAYSIA PAHANG AL-SULTAN ABDULLAH

RESEARCH ARTICLE

Combustion noise characterization and optimization of PCCI combustion using response surface methodology

Y. Datta Bharadwaz[1]*, A. Swarna Kumari[2]

[1] Faculty of Mechanical Engineering, Gayatri Vidya parishad College of Engineering (A), Andhra Pradesh, 530048, Visakhapatnam, India
Phone: +91 9581456166, Fax.: +91-891-2739605
[2] Faculty of Mechanical Engineering, Jawaharlal Nehru Technological University, Andhra Pradesh,533003, Kakinada, India

ABSTRACT - The current work aims at characterizing the premixed charge compression ignition (PCCI) combustion with regression-based approach using response surface methodology. PCCI operating parameters such as load, pilot injection timing, main injection timing, pilot injection quantity, exhaust gas recirculation and injection pressure are considered as input variables. Engine performance indicators such as brake thermal efficiency, brake specific fuel consumption, carbon monoxide (CO), hydrocarbon (HC), oxide of nitrogen (NO_x), smoke emissions, combustion phasing and combustion noise metric ringing intensity are considered as output responses. Experimental results validate the optimal solution from response surface methodology approach, and good agreement is found between mathematical models and experimental results. Comparative examination of optimized PCCI combustion versus conventional combustion showed a 66% and 44% decrement in NO_x and smoke emissions. Except for CO and HC emissions, the percentage penalty of other responses with PCCI combustion is less than 10%. In addition to ringing intensity another combustion noise metric combustion noise level is computed from Fast Fourier Transform (FFT) analysis of cylinder pressure trace. A combustion noise level of 73.26 dB is obtained at optimized conditions.

ARTICLE HISTORY
Received : 18th Mar. 2023
Revised : 01st Oct. 2023
Accepted : 24th Nov. 2023
Published : 26th Dec. 2023

KEYWORDS
PCCI combustion
Optimization
Design of experiments
Response surface methodology
FFT analysis
Combustion noise level

1.0 INTRODUCTION

Growing concerns over diesel engine emissions have led to strict emission standards. These emission standards further complicate the design of diesel engines. Emission compliant architecture of diesel engine often necessities the use of exorbitant after treatment devices. In this scenario, low-temperature combustion concepts are becoming more prominent in diesel engine development as a means for achieving green diesel engines for the present and the future [1–3]. Because of their low emissions and high efficiency, low temperature combustion (LTC) concepts such as homogenous charge compression ignition (HCCI), premixed charge compression ignition (PCCI), and reactivity-controlled compression ignition (RCCI) are being extensively researched. The above combustion concepts showed extremely low NO_x and PM emissions with a remarkable increase in carbon monoxide (CO) and hydrocarbon (HC) emissions. These combustion concepts also suffer from high combustion noise, limited operating range and high cycle-to-cycle variations [4–6]. Many technical solutions, such as alternative fuels, multiple split injections and optimized engine parameters, are proposed to reduce the drawbacks in PCCI combustion [7–10]. To anticipate and improve the operating parameters of diesel engines, a variety of techniques are used, including response surface methodology (RSM), Taguchi-Grey relational analysis, genetic algorithms, particle swarm optimization, artificial neural networks, and fuzzy logic [11–13]. Many researchers used the techniques described above to explore the influence of optimized parameters on diesel engines. In the recent literature, these optimization methodologies are extended to LTC concepts for efficient combustion control. Taguchi-Grey relational analysis is implemented to enhance PCCI-DI combustion. The authors used ANOVA and Grey relational analysis (GRA) to identify optimal combinations of input parameters for diesel engine powered by air blast-injected methanol and diesel. The experiments on optimum input combinations resulted in a 68.02% reduction in NO_x and a 62.73% reduction in smoke compared to conventional diesel operation [14]. Diesel engine powered with producer gas and biodiesel is optimized using response surface methodology. Results indicated an overall desirability of 0.49 for the optimum input conditions. In their works, authors noticed that RSM efficiently integrates triple-fuel modes in CI engines with optimum conditions [15]. The efficiency of RSM in complicated experimental architectures such as gasifier-diesel engine interface is noticed in the literature [16]. RSM-based models are developed to forecast the engine characteristics and diesel replacement rate for producer gas - diesel fueled diesel engines. The producer gas generated from various biomass sources, which has non-uniform calorific values, is tested for their performance and emissions in diesel engines. The developed RSM models predicted an optimal diesel substitution ratio of 59.04% with producer gas [17]. Parametric-based optimization is executed using RSM on a diesel engine with nickel oxide -neem biodiesel nano fuel. The design of experiment (DoE) L29 array is used to collect experimental data, and compression ratio, injection timing, and pressure are considered inputs for optimization. The authors noticed highest desirability of 0.6198 and the quadratic nature for the modelled responses. The predicted values were validated by confirmation tests, which revealed an error rate between 7

*CORRESPONDING AUTHOR | Y. Datta Bharadwaz| ✉ ydattabharadwaz@yahoo.com

and 4.64 [18]. The effect of multiple split injections, more than five pulses per cycle is investigated. To optimize this injection strategy, KIVA-3V coupled genetic algorithms are utilized. It is identified that multiple split injections provide efficient heat release control and air-fuel mixing in the cylinder [19]. DoE-based experimentation and optimization are performed on various injection strategies for minimizing emissions and understanding various trade-off parameters' interactions. Double pilot, main and after injection strategies remarkably improve NO_x emissions and BSFC-NO_x – EGR trade-off curves, compared with other injection strategies [20]. Full factorial DoE is adopted to optimize the diesel engine fuelled with dual fuel. Compression ratio, fuel injection pressure, and the start of injection timing are inputs, whereas performance and emission parameters are outputs. Authors noticed that compression ratio (CR) of 18.5, injection pressure of 240 bar and injection timing of 24.5º BTDC yielded the highest brake thermal efficiency (BTH) and low HC, CO and smoke emissions [21]. The work on PCCI combustion identified the need for injection strategy optimization for the complete utilization of combustion chamber space. The authors noticed an increase in turbulence duration and enhanced mixing in the cylinder for optimized multiple injection strategies. The optimum multiple injection strategies resulted in a drop in NO_x and soot emission by 59.3% and 70.4%, respectively, with a slight increase in indicated thermal efficiency by 0.33% at high speeds [22]. A DoE-RSM-based optimization approach is employed to determine the operational limit and design space of PCCI and RCCI modes of combustion. Optimization results indicated that the split injection strategy is best for emissions and engine performance improvement. The predicted optimum values of the RSM approach with the highest ethanol share showed a notable rise in equivalent brake-specific energy consumption, HC and COV_IMEP [23].

The literature review shows that most works on optimizing diesel engines focus on conventional combustion. Most recent works on engine optimization have identified RSM as an efficient engine optimization and response prediction tool. Significant optimization works in the literature are limited to engine performance and emission parameters. Only few articles have focused on optimizing the LTC parameters of diesel engines. The current study conducts a preliminary optimization analysis of premixed charge compression ignition to determine the best operating parameters for efficient premixed combustion and control. In addition to optimization, an FFT-based cylinder pressure analysis at optimized input conditions is performed to determine the combustion noise level for PCCI combustion.

2.0 EXPERIMENTAL SETUP

The current experimental configuration includes a single cylinder four stroke water-cooled diesel engine. To determine torque and power characteristics, the engine is connected to an eddy current dynamometer. For determining the load applied to the engine, the dynamometer is linked to a strain gauge type load cell. Measurements of combustion pressure, airflow, fuel flow, and engine speed, are carried out with a piezo pressure sensor, pressure transmitter, fuel flow transmitter, and a crank angle sensor. The "National Instruments" high-speed data acquisition system is used to integrate all sensors to a computer. The engine's performance is analysed online using Lab-view based software. In addition to the electronic sensors, the engine has a control cabinet with a fuel-measuring burette, an airflow manometer, and a rotameter for fuel, air and coolant flow measurement. The engine is also linked to a two-stage cooled EGR system with a mechanical valve that can vary EGR from 0 to 30%. To measure the exhaust gas flow rate, an orifice metre is installed in the EGR circuit. Engine coolant temperature, lubricant temperature, intake air temperature, and exhaust gas temperature are measured by using thermocouples installed at various locations throughout the engine test rig. A common rail diesel injection system with rail pressure sensors, a high-pressure fuel pump, and pressure regulators is also integrated with the engine for electronic fuel injection. A dedicated injection driver kit manipulates the injection parameters as per requirement, which include injection pressure, timing, the number of injection events, the amount of injection, and the duration of the injection. An INDUS five-gas analyser and an INDUS smoke metre are used for emission analysis. Figure 1 depicts a simple schematic diagram of the experimental setup and Table 1 shows the engine test rig specifications.

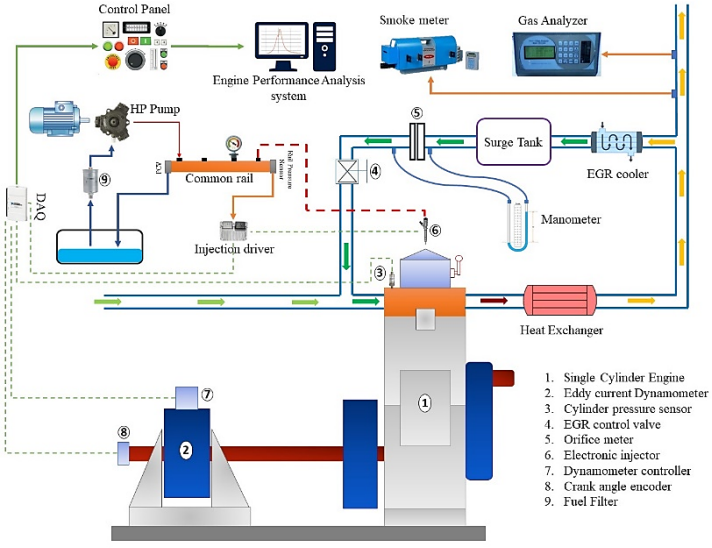

Figure 1. Schematic layout of the engine test setup

Table 1. Engine test rig specifications

Parameter	Specification
Engine make and model	Kirloskar TV1
Engine type	4- stroke, Single cylinder, water-cooled engine, medium speed, direct injection
Bore	87.5 mm
Stroke	110 mm
Swept Volume	661 cc
Rated power	3.5 kW @ 1500 rpm
Compression ratio	18:1
Opening of the inlet valve	4.5° before TDC
Closing of the inlet valve	35.5 ° after BDC
Opening of the exhaust valve	35.5 ° before BDC
Closing of the Exhaust valve	4.5° after TDC
Injector	Bosch
Injection pressure range	200-1100 bar
EGR range	0-30%

Experimentation is conducted at constant intake and lubricating oil temperatures with conventional high-speed diesel (IS 1460) as fuel. Constant engine speed of 1500 rpm is maintained for all testing conditions of the engine. The coolant outlet temperature is maintained at 60°C for all test conditions to achieve steady state operation. Early fuel injection strategies and EGR are employed in the present study to achieve effective PCCI combustion [24–29]. According to the combustion analysis techniques outlined by Richard Stone, the combustion pressure acquired from the piezo sensor is used to compute the fraction of fuel mass burned, net heat release rates, pressure rise rate, and cumulative heat release rates [30]. The uncertainties associated with various measured and derived parameters for the experimental range are calculated using the uncertainty analysis mentioned by Holman [31]. The observed overall uncertainty in the present work is 5.58%, which is comparable to the overall uncertainty observed in existing engine experimental literature [32]. The ringing intensity is considered as a noise metric for estimating the engine cylinder's combustion noise. In addition to the ringing intensity, combustion noise level is computed for the optimized test condition using the FFT analysis of the engine cylinder pressure trace. In the present work, PCCI combustion control inputs such as load, SoPI, SoMI, QSoPI, EGR and injection pressure are taken as numeric factors. Engine performance and combustion indicators such as BTH, BSFC, CO, HC, NOx, smoke emissions, combustion phasing (CA50) and ringing Intensity (RI) are considered responses. Using "Design Expert" software and the face central composite designs, 86 experimental runs are designed in which each parameter varies in three levels. Analysis of designed experiments resulted in a FDS score 0.82, indicating that the present experimental design can be used for analysis and optimization. All experiments are performed according to the run order of the experimental design. The sequence of steps followed for optimization of PCCI combustion is shown in the Figure 2.

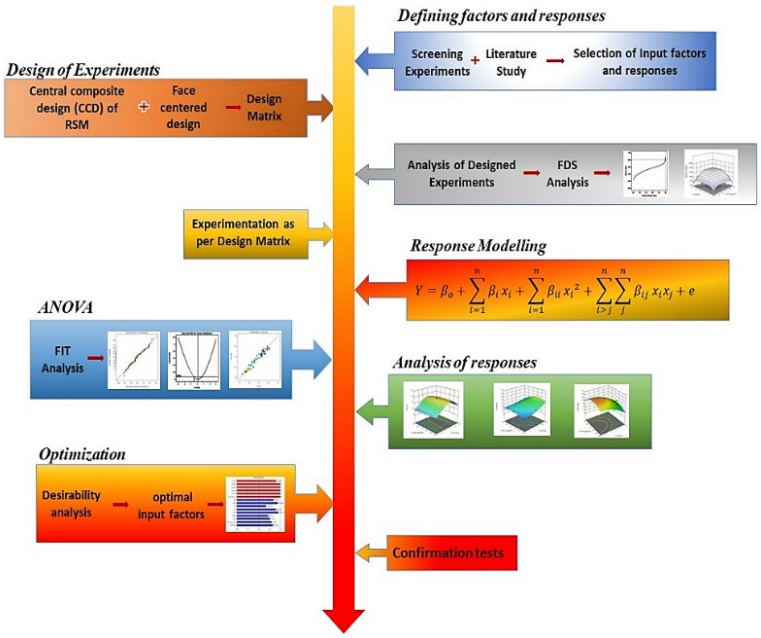

Figure 2. Sequence of response surface methodology

2.1 Response Surface Methodology

It is a statistical and mathematical tool to study and optimize the relationship between different factors. It facilitates the analysis of input factors' effect on responses with quadratic or cubic models. RSM helps to build appropriate empirical models and exploit them for further analysis to understand the relationships among various factors and responses. RSM with proper DoE can generate models which can relate the "n" number of input parameters with responses [33, 34]. The regression equations developed for predicting responses from input factors using response surface methodology are shown from equation 1 to equation 8. The equations are shown in terms of coded factors: A-load, B- SoPI, C-SoMI, D-QSoPI, E-EGR and F-injection pressure. Various transformations are applied to the responses in the present study to improve the fit of the data to the model. The most appropriate transformation for a particular response is selected using box-cox plot.

$$\begin{aligned}\ln(BTH) = {} & 2.92549 + 0.155218 \times A - 0.0286667 \times B + 0.0756902 \times C + 0.016226 \times D \\ & - 0.0116289 \times E - 0.0110482 \times F + 0.0178446 \times AB + 0.0957705 \times AC \\ & + 0.0500783 \times AD + 0.0226009 \times AE - 0.025367 \times AF \\ & + 0.0285147 \times BC + 0.024916 \times BD + 0.0256217 \times CE \\ & + 0.0312124 \times CF - 0.0535633 \times EF - 0.494406 \times A^2\end{aligned} \tag{1}$$

$$\begin{aligned}\ln(BSFC) = {} & -0.799231 - 0.159966 \times A + 0.0294816 \times B - 0.0501521 \times C \\ & - 0.00100213 \times D + 0.0239043 \times E + 0.0339816 \times F - 0.0859158 \times AC \\ & - 0.0416902 \times AD + 0.0216336 \times AF - 0.0277641 \times BC \\ & - 0.0233944 \times BD - 0.0315749 \times CE - 0.0386206 \times CF + 0.048941 \times EF \\ & + 0.55002 \times A^2 + 0.105142 * B^2 - 0.169881 \times F^2\end{aligned} \tag{2}$$

$$\begin{aligned}\ln(CO) = {} & 3.35511 + 0.407604 \times A + 0.0447086 \times B + 0.00737771 \times D + 0.104807 \times E \\ & + 0.0450191 \times F - 0.204182 \times AB + 0.0583626 \times AE + 0.0542777 \times AF \\ & - 0.0497963 \times BD - 0.0450843 \times BE + 0.0605875 \times BF \\ & + 0.0569459 \times EF - 0.335274 \times B^2\end{aligned} \tag{3}$$

$$\begin{aligned}\ln(HC) = {} & -0.893727 + 0.474534 \times A + 0.0346879 \times B - 0.0725776 \times C \\ & - 0.0227461 \times D + 0.207412 \times E - 0.10075 \times F - 0.174047 \times AB \\ & - 0.171908 \times AC - 0.144865 \times AD + 0.0796133 \times AE - 0.0705244 \times BC \\ & - 0.0639451 \times BD - 0.0882477 \times BE - 0.0780611 \times CE \\ & + 0.159462 \times EF + 0.524909 * A^2\end{aligned} \tag{4}$$

$$\begin{aligned}\sqrt{NO_x} = {} & 1.29127 - 0.721828 \times A - 0.321737 \times B + 0.557497 \times C + 0.157363 \times D \\ & - 0.529614 \times E - 0.234815 \times F + 0.118677 \times AB - 0.278006 \times AC \\ & + 0.192979 \times AD + 0.303483 \times AF - 0.0837331 \times BC - 0.149483 \times EF \\ & + 0.447173 \times A^2 + 0.432017 \times F^2\end{aligned} \tag{5}$$

$$\begin{aligned}Smoke = {} & 56.3 + 6.74242 \times A - 1.07576 \times C + 0.151515 \times D + 1.12121 \times E \\ & + 2.22727 \times F + 1.09375 \times AC + 0.3125 \times AD - 0.4375 \times AE \\ & + 0.78125 \times AF - 0.375 \times DE + 0.46875 \times DF + 1.83636 \times C^2\end{aligned} \tag{6}$$

$$\begin{aligned}CA50 = {} & 54.7123 - 14.3333 \times A - 1.36364 \times B + 0.272727 \times C - 0.181818 \times D \\ & - 1.10606 \times E + 0.636364 \times F + 1.875 \times AB + 2.78125 \times AE \\ & - 5.3125 \times AF - 2.03125 \times CD - 3.25 \times CE - 2.28125 \times CF \\ & - 2.40625 \times EF - 6.62318 \times A^2 - 13.6232 \times B^2\end{aligned} \tag{7}$$

$$\begin{aligned}\ln(RI) = {} & 2.15064 + 0.382031 \times A - 0.113481 \times B + 0.388394 \times C + 0.00297062 \times D \\ & - 0.0181381 \times E - 0.0971461 \times F + 0.0824557 \times AD + 0.146364 \times AE \\ & + 0.239661 \times AF - 0.07473 \times CD - 0.0999117 \times CE - 0.101385 \times CF\end{aligned} \tag{8}$$

2.2 Model evaluation using ANOVA

ANOVA analyses and tests the generated regression models for their statistical validity. The ANOVA analysis parameters such as P-value, F- value, R^2, R^2 adjusted and Predicted R^2 indicate the significance of the developed models. The closeness of R^2 and R^2 adjusted to one indicates precession of model fit, and agreement between predicted R^2 and adjusted R^2 shows that the model fits the data. A difference less than 0.2 between R^2 adjusted and R^2 predicted is usually considered reasonable agreement to interpolate the model [35]. The difference between the R^2 adjusted and R^2 predicted greater than 0.2 indicates problems with the model or the input data. The R^2 values for all the responses are higher than 0.8 as shown in Table 2, representing a good fit of the experimental data to the model. The difference between R^2 adjusted and R^2 predicted is less than 0.2 for all the responses shown in Table 2. The f-value and p-value indicate the significance of the model and model terms. The model terms with a P-value less than 0.05 are considered significant, whereas the model terms with a P-value greater than 0.05 are considered insignificant. The model with a larger F-value is usually

considered significant in the present analysis [36]. The P-values for all the response models are less than 0.0001, exhibiting the data fitting with mathematical models. In the present study, quadratic models are selected for all responses except for ringing intensity (RI), and cubic models are aliased for all the responses. Significant model terms (P>0.05) are considered using reduced models to improve the accuracy. Adequate precision is an indicator which depicts the signal-to-noise ratio, and a value higher than four indicates an adequate signal. The value of adequate precision for all the responses is greater than four, as shown in Table 2.

Table 2. ANOVA analysis and fit statistics of responses

	BTH	BSFC	CO	HC	NO_x	Smoke	CA50	Ringing Intensity
Transformation	Natural log	Natural log	Natural log	Natural log	Square Root	-	-	Natural log
Model	Reduced Quadratic	Reduced Quadratic	Reduced Quadratic	Reduced Quadratic	Reduced Quadratic	Reduced Quadratic	Reduced Quadratic	Reduced 2FI
Sum of squares for Model	7.03	6.87	17.49	31.74	112.62	3697.60	23897.42	28.22
df	17	17	13	16	14	12	15	12
F-value	72.89	45.99	29.78	25.85	57.09	149.82	27.15	27.77
p-value	<0.0001	<0.0001	<0.0001	<0.0001	<0.0001	<0.0001	<0.0001	<0.0001
R^2	0.95	0.92	0.84	0.86	0.92	0.96	0.85	0.82
Adjusted R^2	0.93	0.90	0.81	0.82	0.90	0.95	0.82	0.79
Predicted R^2	0.90	0.86	0.77	0.77	0.88	0.95	0.77	0.75
Adequate precision	26.68	24.33	21.68	24.33	32.64	41.57	18.46	19.13

3.0 RESULTS AND DISCUSSION

The impact of PCCI combustion on engine operational and emissions indicators such as BTH, BSFC, CO, HC, NO_x, Smoke, CA50 and ringing intensity are analysed using response surface plots. The safe operational limits of the engine with PCCI combustion are also identified with response surface analysis. The effect of each input factor on responses is discussed below.

3.1 Brake Thermal Efficiency

The interaction effect of load, injection parameters and EGR on brake thermal efficiency is shown in Figure 3. Figure 3a shows an increase in thermal efficiency with load, and a drop in thermal efficiency is observed at higher loads. Increase in EGR has shown detrimental effects on brake thermal efficiency. This effect is predominant at lower loads due to lower combustion temperature and increased dilution effect of EGR [37]. The influence of the SoPI and SoMI on brake thermal efficiency is shown in Figure 3(b). Advancing the SoMI beyond 20^o BTDC showed improved thermal efficiency in the selected range of pilot injection timings. Retarded main injection decreased the thermal efficiency for the same SoPI. Pilot injection timings greater than 50^o BTDC are required to maintain the brake thermal efficiency for retarded main injections. Close placement of SoMI and SoPI timings resulted in a knock and drop in thermal efficiency. The influence of IP and SoMI on brake thermal efficiency is shown in Figure 3(c). The Figure 3(c) shows increased IP has improved the BTH [38]. Injection pressure above 300 bar and SoMI greater than 23^{o}BTDC range enhanced the BTE of the engine. The impact of QSoPI and the SoPI is shown in Figure 3(d). The increase in QSoPI at very advanced SoPI timings decreased thermal efficiency. In contrast, brake thermal efficiency increased slightly with the QSoPI for SoPI timings less than 65^o BTDC. For optimal brake thermal efficiency with PCCI combustion, the operating limits of the engine are identified as load <60%, 20^o BTDC < SoMI <25^o BTDC, 40^o BTDC< SoPI < 60^o BTDC, injection pressure > 300 bar, 5%< EGR< 15%, 5%< Q.SoPI< 10%.

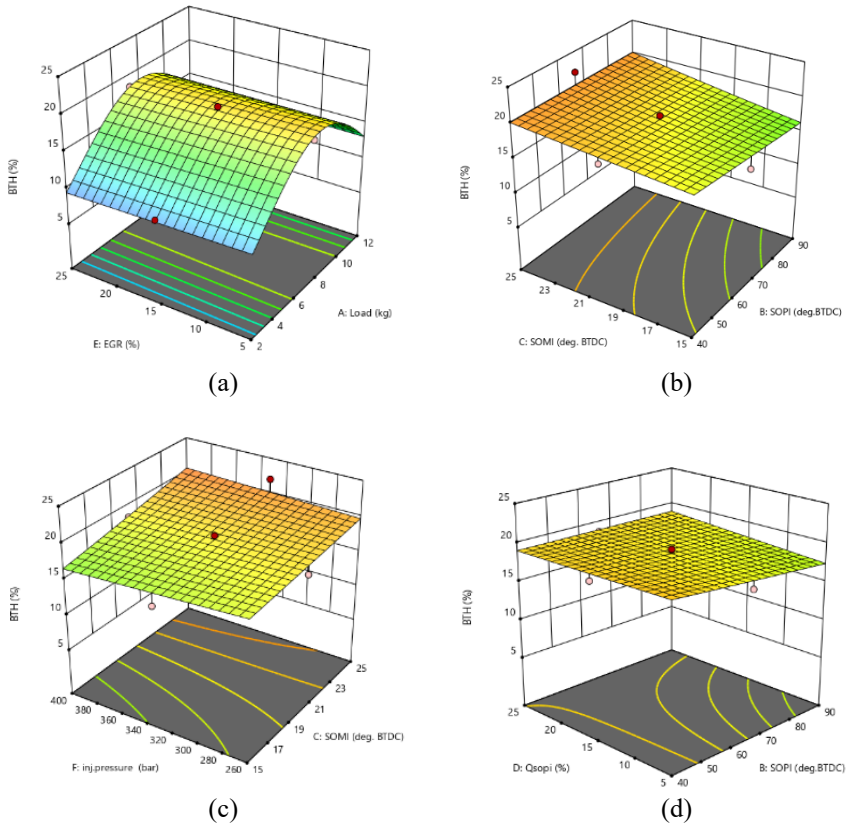

(a) (b)

(c) (d)

Figure 3. Interaction effect of brake thermal efficiency with: (a) Load and EGR, (b) SoPI and SoMI, (c) injection pressure and SoMI and (d) Q.SoPI and SoPI

3.2 Brake Specific Fuel Consumption

Figure 4 depicts the interaction effects of BSFC with various input factors. Figure 4(a) depicts the effect of load and SoMI on BSFC.BSFC, like BTH, is lowest between 45% and 75% of the load. The advancement of SoMI from 15° BTDC to 25° BTDC showed a drop in BSFC [39]. The effect of SoMI and SoPI on BSFC is shown in Figure 4(b). Advancement of pilot injection timing to 90° BTDC and retardation of pilot injection timing to 40° BTDC showed increased brake specific fuel consumption. In contrast, pilot injection timing from 60°-70° BTDC showed the lowest BSFC [40]. The impact of injection pressure and EGR on BSFC is showcased in Figure 4(c). The rise in % EGR increased BSFC and is highest at 25% EGR. The increase in injection pressure decreased BSFC and is identified to be lowest at 400 bar. The effect of QSoPI and SoPI on brake specific fuel consumption is shown in Figure 4(d). With the increase in QSoPI, there is a slight increase in BSFC. The best range of engine operational parameters for BSFC are load <60%, 20° BTDC < SoMI <25° BTDC, 60° BTDC< SoPI < 70° BTDC, injection pressure > 300 bar, 5%< EGR< 15%, 5%< Q.SoPI< 10%.

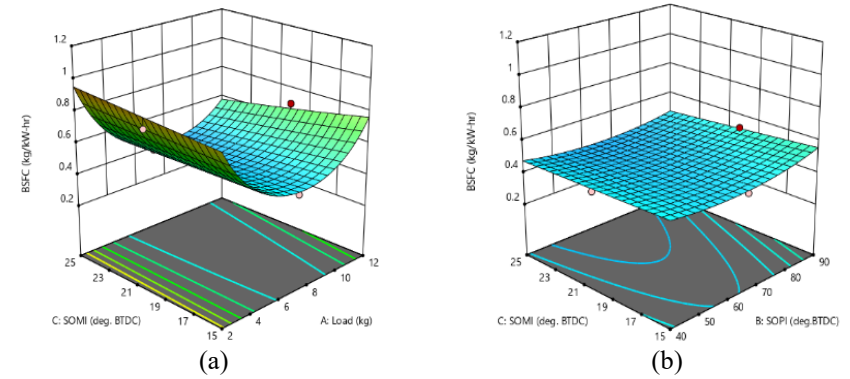

(a) (b)

Figure 4. Interaction effect of brake specific fuel consumption with: (a) Load and SoMI, (b) SoPI and SoMI,

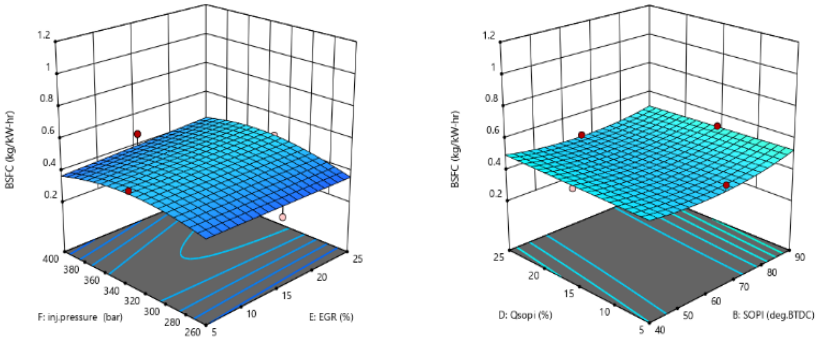

(c) (d)

Figure 4. (cont.) (c) injection pressure and EGR and (d) Q.SoPI and SoPI

3.3 Carbon Monoxide Emissions

The impact of different PCCI combustion factors on CO emissions is shown in Figure 5. The influence of load and SoPI on CO emissions is shown in Figure 5(a). A dramatic rise in CO emissions is observed for PCCI combustion. This is due to the early fuel injections and lower temperatures prevailing at earlier stages of compression stroke [39], [41]. A rise in CO emissions is observed with the rise in load. CO emission dropped with retarded pilot injections and increased with advanced pilot injections. The identical behaviour of CO emissions with retarded pilot injections is noticed by Kaiadi et al. in their works [42]. Figure 5(b) depicts the outcomes of SoPI and EGR on CO emissions. The rise in EGR caused a rise in CO emissions. EGR less than 15% emits less CO than EGR greater than 15%. The combined effects of load and IP on CO emission are presented in Figure 5(c). The rise in IP has a slight incremental effect on CO emissions. The effect of QSoPI on CO emissions is showcased in Figure 5(d). An increment in pilot injection quantity has increased CO emissions. The pilot injection quantity of less than 15% has lower CO emissions. For minimum CO emissions, the operating range of input factors is found to be load <50%, 20º BTDC < SoMI <25º BTDC, 40º BTDC< SoPI < 50º BTDC, injection pressure < 300 bar, 5%< EGR< 15%, 5%< Q.SoPI< 10%.

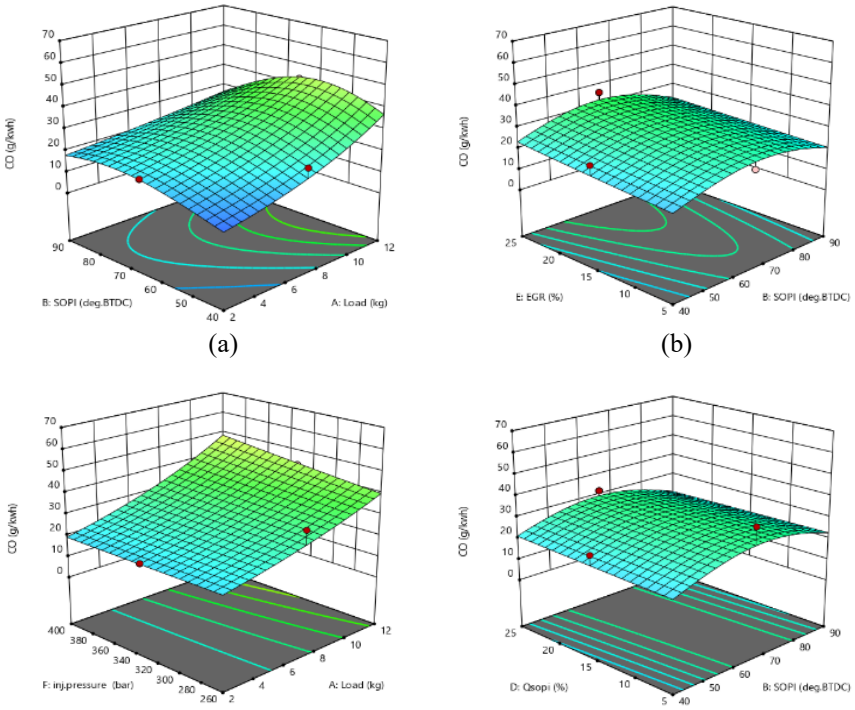

(a) (b)

(c) (d)

Figure 5. Interaction effect of carbon monoxide emissions with: (a) Load and SoPI, (b) SoPI and EGR, (c) injection pressure and load, (d) Q.SoPI and SoPI

3.4 Hydrocarbon Emissions

In PCCI combustion, the early injection strategy increases the unburned hydrocarbon emissions due to the wall-wetting phenomena [2]. The impact of PCCI combustion on HC emissions with various interaction effects of parameters is shown in Figure 6. The effect of SoMI and SoPI timings on HC emissions is showcased in Figure 6(a). From the Figure 6a, it is identified that there is an increment in HC emissions with the advancement of SoPI timings from 40º BTDC to 90º BTDC. However, HC emission decreases with the advancement of SoMI from 15º BTDC to 25º BTDC. Like CO emissions, HC emissions increased with the load, as shown in Figure 6(b). The Figure 6(b) also revealed that increasing

the QSoPI at low loads increased HC emission. At high loads, increasing the QSoPI reduced the HC emissions. This is due to the high temperature and pressures at higher engine loads facilitating HC oxidation. Figure 6(c) shows that increase in EGR results in rise of HC emissions. This rise in HC emissions caused by EGR is highest at higher loads. In all engine operating conditions, increasing injection pressure resulted in lower HC emissions. The optimum range of input parameters for low HC emissions are load <50%, 21° BTDC < SoMI <25° BTDC, 40° BTDC< SoPI < 65° BTDC, injection pressure > 300 bar, 5%< EGR< 15%, 5%< QSoPI< 10%.

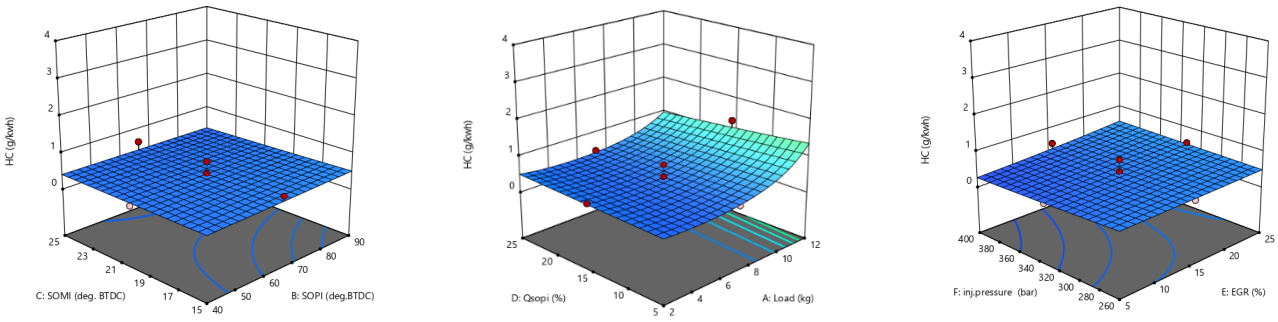

(a) (b) (c)

Figure 6. Interaction effect of hydrocarbon emissions with: (a) SoMI and SoPI, (b) Q. SoPI and load, (c) injection pressure and EGR and (d) QSoPI and SoPI

3.5 NO_x Emissions

PCCI combustion results in decreased NO_x emissions in comparison with regular combustion due to the lower cylinder temperatures [38, 43]. The influence of various input factors on NO_x emissions is presented in Figure 7. The effect of load and SoMI on NO_x emissions is exhibited in Figure 7(a). Owing to PCCI combustion, very low NO_x emissions are noticed in the experiments as shown in response plots. Advancement of SoMI and increasing load resulted in increased NO_x emissions. The influence of EGR and IP on NO_x emission is showcased in Figure 7(b). Increased NO_x emissions with an increase in IP and decreased NO_x emissions with rise in EGR is noticed from Figure 7(b). The NOx emissions decreased with increased EGR due to the increased heat carrying capacity of gases and decreased cylinder temperatures. Increased injection pressure increases atomization and mixing, increasing cylinder temperature and NO_x emissions. As shown in Figure 7(c), the rise in pilot injection quantity increased NO_x emissions. This effect is the result of abrupt burning of accumulated fuel in the premixed combustion phase causing cylinder temperatures to rise. The interaction effects of SoPI timing and SoMI on NO_x emissions are shown in Figure 7(d). Advancing the SoPI has shown decrement in NO_x emissions. The range of input parameters for lower NO_x emissions is 40%<load <50%, 15° BTDC < SoMI <20° BTDC, 65° BTDC< SoPI < 90° BTDC, 300 < injection pressure > 360 bar, 15%< EGR< 25%, 5%< Q.SoPI< 10%.

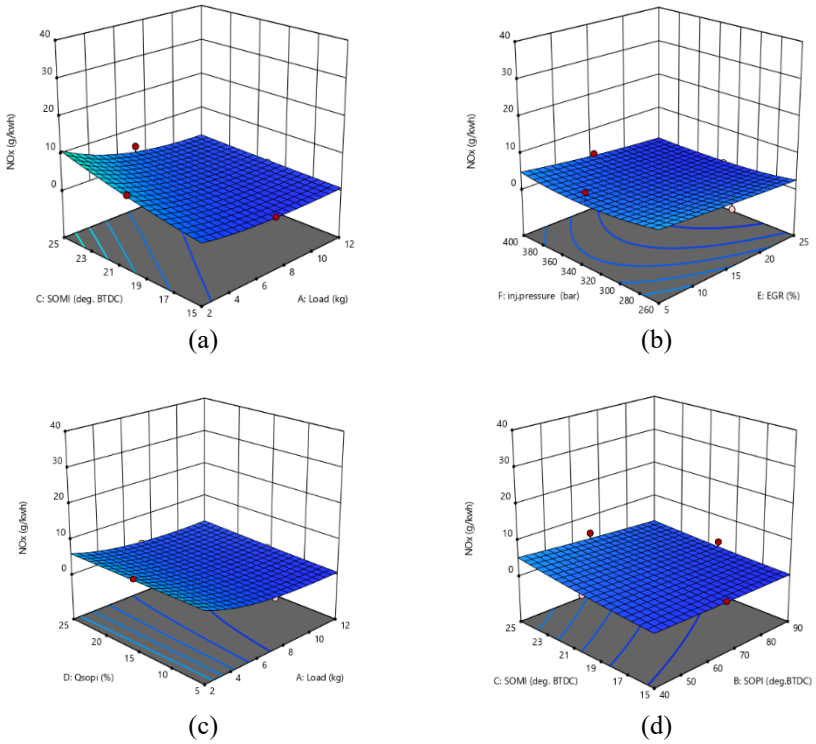

(a) (b)

(c) (d)

Figure 7. Interaction effect of NO_x emissions with: (a) Load and SoMI, (b) Injection pressure and EGR, (c) Q.SoPI and Load and (d) SoPI and SoMI

3.6 Smoke Emissions

The influence of input factors and corresponding interaction effects on Smoke emissions is showcased in Figure 8. Figure 8(a) shows that smoke emissions increase with load. As shown in Figure 8(a), as main injection advancement increases, smoke emissions decrease. This decrease in smoke emissions with injection advancement is due to premixed combustion [39, 41]. The dual effect of EGR and QSoPI on smoke is showcased in Figure 8(b). The figure shows a rise in smoke emission with increased EGR% and QSoPI [44]. The impact of IP on smoke emissions is presented in Figure 8(c). The figure depicts that increased IP results in slightly increased smoke emissions. The best range of operating conditions for minimum smoke emissions are found to be load<40%, 21° BTDC < SoMI <25° BTDC, 300 < injection pressure > 360 bar, 5%< EGR< 15%, 5%< Q.SoPI< 10%.

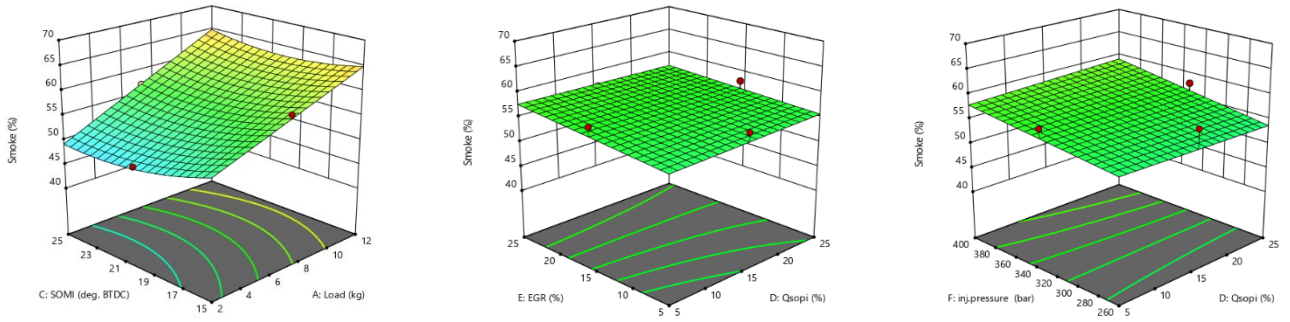

(a) (b) (c)

Figure 8. Interaction effect of Smoke emissions with: (a) SoMI and Load, (b) Q.SoPI and EGR, and (c) injection pressure and Q.SoPI

3.7 Combustion Phasing (CA50)

Combustion phasing, play a vital role influencing the engine's performance. Improper phasing of CA50 results in loss of thermal efficiency and knocking [45–47] The effect of various input factors on CA50 is shown in Figure 9. From Figure 9(a), advancement in CA50 with increase in load and retardment with a decrease in load is identified. This phenomenon is because of the increased temperature and pressure enhancing the combustion at high loads. Observations from the Figure 9(a) also indicated that advancing the SoPI retards the CA50, whereas retarding the SoPI advances the CA50. Very advanced SoPI results in wall wetting and slow fuel burning [48]. Figure 9(b) shows the impact of SoMI and QSoPI on combustion phasing. The CA50 angle was farther from TDC when the main injection time was delayed, but it was closer to TDC when it was advanced to 25° BTDC. This phenomenon is due to enhanced premixed combustion at advanced main injection timings. The work of Das et al. on HCCI combustion observed a similar occurrence with retarded SoMI [49]. Figure 9(b) manifests that increasing the QSoPI by more than 15% shifts the CA50 away from TDC. Figure 9(c) depicts the influence of IP and EGR on CA50. The increase in IP resulted in a slightly delayed combustion phase, while the increase in EGR resulted in little progress in the combustion phase. The range of operating parameters for the best combustion phase from response plot analysis is 40%<load<80%, 21° BTDC < SoMI <25° BTDC, 300 < injection pressure < 330 bar, 15%< EGR< 25%, 5%< Q.SoPI< 15%.

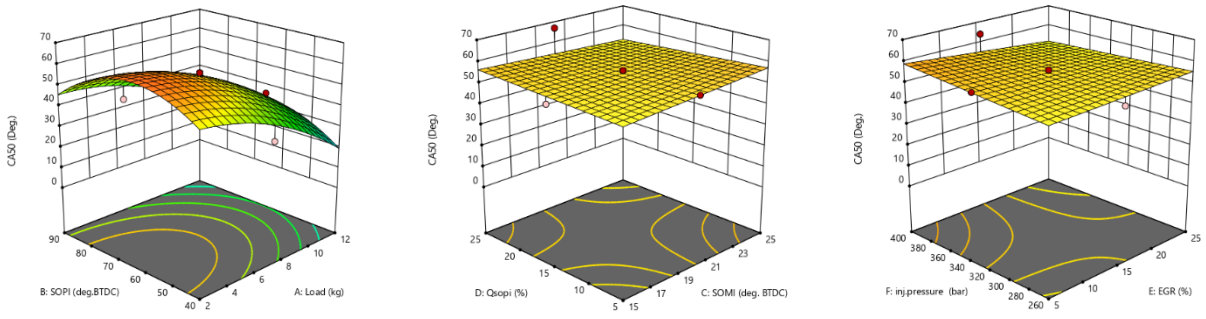

(a) (b) (c)

Figure 9. Interaction effect of combustion phasing with: (a) SoPI and Load, (b) Q.SoPI and SoMI, and (c) injection pressure and EGR

3.8 Ringing Intensity

In premixed combustion, all the fuel is injected before combustion, which would result in severe knocking. Because of this, ringing intensity become a vital parameter in PCCI combustion and impose limits on the load and injection parameters. In the present work, a ringing intensity of 5MW/m^2 is the maximum limit beyond which the engine tends to knock [50, 51]. The interaction effect of ringing intensity with various input factors is shown in Figure 10. The impact of load and QSoPI on ringing intensity is shown in Figure 10(a). The ringing intensity increased with the rise in load. This is on account of the rise in cylinder pressures and rate of pressure rise with the increment in load. From the figure, the

increase in QSoPI increased the ringing intensity. The increase in QSoPI resulted in a drastic pressure rise rate increasing the ringing intensity. The influence of the SoMI and EGR on ringing intensity is shown in Figure 10(b). The main injection advancement increased ringing intensity. This effect is due to the increased premixed combustion mode with injection advancement. A decrease in ringing intensity is noticed with an increase in EGR. The increase in EGR was found to have decreased the cylinder temperatures resulting in lower cylinder pressures. Figure 10(c) depicts the effect of IP and SoMI on ringing intensity. Figure 10(c) also indicates an increase in ringing intensity as injection pressure is increased. This is due to the enhanced combustion and rise in the cylinder pressures. The suitable operating range for optimum ringing intensity is identified as load<40%, 15° BTDC < SoMI <20° BTDC, 40° BTDC < SoPI <65° BTDC, 300 < injection pressure < 330 bar, 15%< EGR< 25%, 5%< Q.SoPI< 15%.

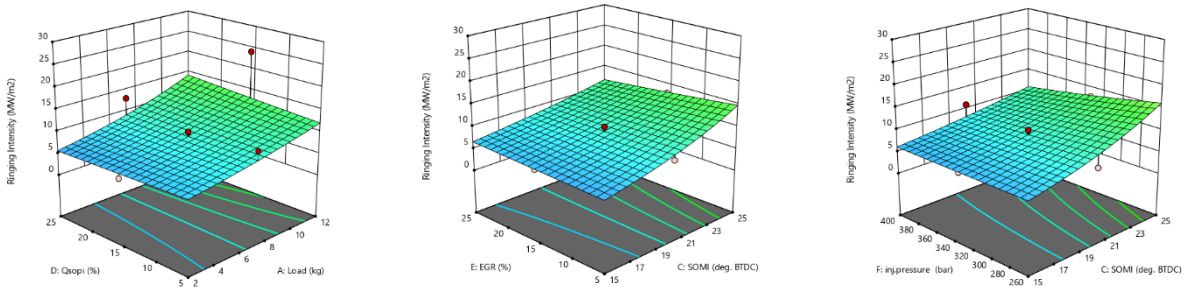

(a) (b) (c)

Figure 10. Interaction effect of ringing intensity: (a) Q.SoPI and Load, (b) EGR and SoMI, and (c) injection pressure and SoMI

3.9 Optimization Criteria

The various input factors are optimized using desirability approach of RSM. In the desirability approach, each response parameter can be assigned a goal of maximize and minimize. Each response is assigned weights and importance based on the optimization criteria [52]. The optimization criteria used in the present study for different responses are presented in Table 3. The input factors are given the importance of three, and the output responses are given the importance of five. When choosing the optimization criteria, a trade-off relation is observed between the different responses. Different weights in the range of 0.1-1 are assigned to different responses to achieve an optimum set of input parameters. Desirability approach of RSM is implemented for optimizing the multiple objectives. The desirability approach results in a set of solutions for the multi-objective optimization of various input factors. The solution with the highest desirability value of 0.73 is chosen as the optimal solution. The best combination of input parameters is 6 kg load (which is 50% of full load), 40° BTDC SoPI, 15° BTDC SoMI, 5% pre-injection, 5% EGR and an IP of 328 bar. The responses at best input combinations are 18.9% BTH, 0.47 kg/kWh BSFC, 14 g/kWh CO, 0.22 g/kWh HC, 2.33 g/kWh NOx, 56% smoke opacity, 41° ATDC CA50 and 5 MW/m^2 RI.

Table 3. Optimization criteria

Name	Goal	Lower	Upper	Lower	Upper	Importance
A: Load (kg)	maximize	2	6	0.1	1	3
B: SOPI (°BTDC)	is in range	40	90	1	1	3
C: SOMI (°BTDC)	is in range	15	25	1	1	3
D: QSoPI (%)	is in range	5	25	1	1	3
E: EGR (%)	is in range	5	25	1	1	3
F: inj. pressure (bar)	maximize	260	400	0.5	1	3
BTE (%)	maximize	7.98	22.03	1	1	5
BSFC (kg/kWh)	minimize	0.3	1.07	1	0.1	5
CO (g/kWh)	minimize	6.75	65.8	0.1	1	5
HC (g/kWh)	minimize	0.11	3.3	0.1	1	5
NOx (g/kWh)	minimize	0.06	34.18	0.1	0.1	5
Smoke (%)	minimize	43	70	1	1	5
CA50 (°BTDC)	minimize	6	50	1	0.5	5
Ringing Intensity (MW/m^2)	minimize	2	26	0.5	0.5	5

3.10 Validation

Triplicate experiments are performed with the optimal combination of input factors to validate the model. The mean response values from triplicate experiments are compared to the prediction interval, as shown in Table 4. The observed mean of the confirmation experiments is within the confidence interval. This occurrence ensures that the developed model

is statistically secure. The maximum error between the predicted and experimental mean is less than 10%, confirming that the mathematical models agree with the experimental results. The optimized PCCI combustion responses obtained from the response surface methodology are compared with conventional combustion. Results indicated a 66% drop in NOx and 44% drop in soot emissions with a penalty in BTH, CO, HC and RI. Except for CO and HC emissions, the penalty in other responses is found to be less than 10%.

Table 4. Confirmation tests

Response	Predicted Mean	95% PI low	Experimental Mean	95% PI high	Error (%)
BTH (%)	18.95	17.16	20.04	20.79	-5.4
BSFC (kg/kWh)	0.47	0.4	0.44	0.55	6.8
CO(g/kWh)	14.62	11.14	15.68	18.32	-6.8
HC (g/kWh)	0.23	0.15	0.25	0.32	-8
NOx (g/kWh)	2.44	1.11	2.47	3.91	-1.2
Smoke (%)	56.36	54.72	55.5	58	1.5
CA50 (^{o}BTDC)	42	29.8	40.5	53.27	3.7
Ringing Intensity (MW/m^2)	5.45	3.82	5.07	7.63	7.5

3.11 Combustion Noise Level

In addition to the ringing intensity, the present study calculates the combustion noise level under optimized conditions. The time-domain-based cylinder pressure curve is converted into a frequency domain using FFT and to combustion noise level using an algorithm proposed by Shahlari et al. [53]. The structural attenuation (SA) and filter corresponding to the human ear response, A, are applied. The exemplary PSD of the cylinder pressure with combined structural attenuation and A- filter is shown in Figure 11. The RMS value of the filtered pressure curve with a reference sound level of $20\mu Pa$ is used to calculate the engine combustion noise using equation 9. The combustion noise level is computed for cylinder pressures of 10 cycles and averaged to get the final readings [50]. The combustion noise level under optimized conditions is determined to be 73.26 dB from the FFT-based analysis.

$$CNL(dB) = 20 \times log_{10}\left(\frac{P_{RMS}}{20_{\mu Pa}}\right) \tag{9}$$

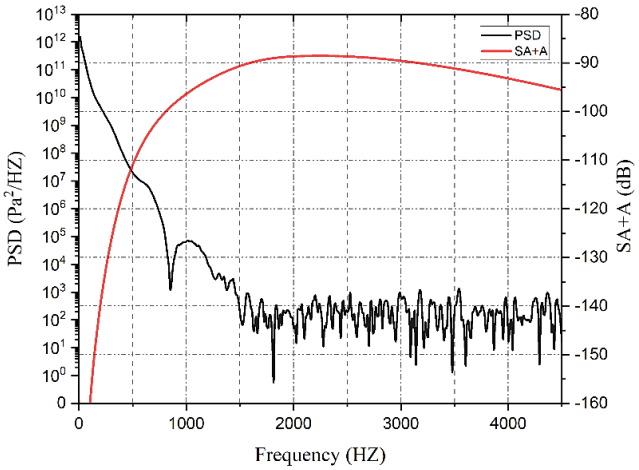

Figure 11. Power spectral density spectrum of cylinder pressure at optimized conditions with combined structural attenuation and A-filter

4.0 CONCLUSIONS

Experimental investigation and optimization analysis are performed on PCCI combustion with double injection strategy using DoE and response surface methodology. From the experimental and statistical examination of the results, the following inferences are drawn.

1) Experimental design and response surface methodology have proven to be excellent tools for analyzing and optimizing low-temperature combustion techniques like PCCI. RSM's face-centered CCD designs have an FDS of 0.82, indicating a good design for PCCI parameter modelling.

2) ANOVA analysis of different responses revealed R^2 values greater than 0.8, indicating that the generated mathematical models fit the experimental data well. Each response parameter's response surface analysis identified a suitable operation region for the PCCI combustion.
3) The solution with the desirability value of 0.73 is chosen as the optimal solution with a 6 kg load (which is 50% of full load), 40° BTDC SoPI, 15° BTDC SoMI, 5% pre-injection, 5% EGR and an injection pressure of 328 bar as the optimum input conditions. The response values with optimal input combinations are 18.9% BTH, 0.47 kg/kWh BSFC, 14 g/kWh CO, 0.22 g/kWh HC, 2.33 g/kWh NOx, 56% smoke opacity, 41° ATDC CA50 and 5 MW/m^2 RI.
4) A comparative analysis between optimized PCCI combustion and conventional combustion is carried out. The results showed a parallel reduction in NO_x and soot emissions compared to conventional combustions, and a dramatic rise in CO and HC emissions is observed. The percentage increase in BSFC, CA50 and RI is less than 10% under optimized conditions.
5) An optimal combustion noise level of 73.26 dB is attained using the FFT of the cylinder pressure curve.

Finally, it is noticed that the PCCI combustion can be adequately characterised and optimized using the response surface methodology. Compared to conventional combustion, the penalty of the response such as brake thermal efficiency can be effectively reduced further by optimising the PCCI combustion parameters in conjunction with alternative fuels.

5.0 ABBREVIATIONS

ANN	Artificial neural networks	GRA	Grey relational analysis
ANOVA	Analysis of variance	HC	Hydrocarbon
BDC	Bottom dead centre	IMEP	Indicative mean effective pressure
BP	Brake power	IT	Injection timing
BSFC	Brake specific fuel consumption	IP	Injection pressure
BTDC	before top dead centre	LTC	Low temperature combustion
BTH	Brake thermal efficiency	NO_x	Oxides of Nitrogen
CA50	Combustion phasing angle	PCCI	Premixed charge compression ignition
CD	Combustion duration	PSD	Power spectral density
CNL	Combustion noise level	QSoPI	Quantity of pilot injection
CO	Carbon monoxide	RI	Ringing intensity
COV	Coefficient of variation	ROHR	Peak rate of pressure rise
CR	Compression ratio	RSM	Response surface methodology
CRDI	Common rail diesel injection	RMS	Root mean square
DI	Direct injection	SA+A	Combined Structural attenuation and A-filter
DoE	Design of Experiments	SoMI	Start of main injection timing
EGR	Exhaust gas recirculation	SoPI	Start of Pilot injection timing
EHN	Ethylhexyl nitrate	TDC	Top dead centre
FDS	Fraction of design space		
FFT	Fast Fourier transform		

6.0 CONFLICT OF INTEREST

The authors declare no conflicts of interest.

7.0 ACKNOWLEDGMENTS

The authors would like to thank Prof. Dr. B. Govinda Rao for his magnanimous support in successful completion of this project.

8.0 REFERENCES

[1] A. P. Singh, N. Sharma, V. Kumar, and A. K. Agarwal, "Experimental investigations of mineral diesel/methanol-fueled reactivity-controlled compression ignition engine operated at variable engine loads and premixed ratios," *International Journal of Engine Research*, vol. 22, no. 7, pp. 2375–2389, 2021.

[2] A. K. Agarwal, A. P. Singh, and R. K. Maurya, "Evolution, challenges and path forward for low temperature combustion engines," *Progress in Energy and Combustion Science*, vol. 61, pp. 1–56, 2017.

[3] C. Berggren and T. Magnusson, "Reducing automotive emissions - The potentials of combustion engine technologies and the power of policy," *Energy Policy*, vol. 41, pp. 636–643, 2012.

[4] T. Pachiannan, W. Zhong, S. Rajkumar, Z. He, X. Leng, and Q. Wang, "A literature review of fuel effects on performance and emission characteristics of low-temperature combustion strategies," *Applied Energy*, vol. 251, pp. 113-380, 2019.

[5] R. D. Reitz and G. Duraisamy, "Review of high efficiency and clean reactivity controlled compression ignition (RCCI) combustion in internal combustion engines," *Progress in Energy and Combustion Science*, vol. 46, pp. 12–71, 2015.

[6] M. Krishnamoorthi, R. Malayalamurthi, Z. He, and S. Kandasamy, "A review on low temperature combustion engines: Performance, combustion and emission characteristics," *Renewable and Sustainable Energy Reviews*, vol. 116, pp. 109-404, 2019.

[7] J. Hwang, Y. Jung, and C. Bae, "Biodiesel PCI combustion for performance and emission improvement in a compression ignition engine," *Energy and Fuels*, vol. 35, no. 2, pp. 1523–1534, 2021.

[8] R. Dijkstra, G. di Blasio, M. Boot, C. Beatrice, and C. Bertoli, "Assessment of the effect of low cetane number fuels on a light duty CI engine: Preliminary experimental characterization in PCCI operating condition," *SAE Technical Paper,* no. 2011-24-0053, 2011.

[9] S. K. Pandey, S. R. Sarma Akella, and R. V. Ravikrishna, "Novel fuel injection strategies for PCCI operation of a heavy-duty turbocharged diesel engine," *Applied Thermal Engineering*, vol. 143, pp. 883–898, 2018.

[10] S. D'Ambrosio, D. Iemmolo, A. Mancarella, and R. Vitolo, "Preliminary optimization of the PCCI combustion mode in a diesel engine through a design of experiments," *Energy Procedia*, vol. 101, pp. 909–916, 2016.

[11] D. B. Yellapragada, G. R. Budda, and K. Vadavelli, "Optimization of injection parameters for ethanol blends of plastic oil in VCR engine using RSM and ANN," *World Journal of Engineering*, vol. 18, no. 6, pp. 906–919, 2021.

[12] B. Paramasivam, "Fuzzy prediction and RSM optimization of CI engine performance analysis: Aegle marmelos non-edible seed cake pyrolysis oil as a diesel alternative," *Energy Sources, Part A: Recovery, Utilization and Environmental Effects*, pp. 1-17, 2020.

[13] Y. Li, M. Jia, X. Han, and X. S. Bai, "Towards a comprehensive optimization of engine efficiency and emissions by coupling artificial neural network (ANN) with genetic algorithm (GA)," *Energy*, vol. 225, pp. 1203-1231, 2021.

[14] G. Alemayehu, D. Firew, R. B. Nallamothu, A. Wako, and R. Gopal, "Operating parameters optimization for lower emissions in diesel engine with PCCI-DI mode using Taguchi and grey relational analysis," *Heliyon*, vol. 8, no. 6, pp. 967-969, 2022.

[15] D. Kumar Singh, R. Raj, and J. V. Tirkey, "Performance and emission analysis of triple fuelled CI engine utilizing producer gas, biodiesel and diesel: An optimization study using response surface methodology," *Thermal Science and Engineering Progress*, vol. 36, pp. 1014-10186, 2022.

[16] D. K. Singh and J. V. Tirkey, "Performance optimization through response surface methodology of an integrated coal gasification and CI engine fuelled with diesel and low-grade coal-based producer gas," *Energy*, vol. 238, pp. 1219-1282, 2022.

[17] G. A. Prasad, P. C. Murugan, W. B. Wincy, and S. J. Sekhar, "Response surface methodology to predict the performance and emission characteristics of gas-diesel engine working on producer gases of non-uniform calorific values," *Energy*, vol. 234, pp. 1212-1225, 2021.

[18] C. Srinidhi, A. Madhusudhan, S. V. Channapattana, S. V. Gawali, and K. Aithal, "RSM based parameter optimization of CI engine fuelled with nickel oxide dosed Azadirachta indica methyl ester," *Energy*, vol. 234, pp. 1212-1282, 2021.

[19] Y. Liu and R. D. Reitz, "Optimizing HSDI Diesel Combustion and Emissions Using Multiple Injection Strategies," *SAE Technical Paper*, no. 2005-01-0212, 2005.

[20] S. D'Ambrosio and A. Ferrari, "Potential of multiple injection strategies implementing the after shot and optimized with the design of experiments procedure to improve diesel engine emissions and performance," *Applied Energy*, vol. 155, pp. 933–946, 2015.

[21] N. Khayum, S. Anbarasu, and S. Murugan, "Optimization of fuel injection parameters and compression ratio of a biogas fueled diesel engine using methyl esters of waste cooking oil as a pilot fuel," *Energy*, vol. 221, p. 119865, 2021.

[22] Y. Lu, C. Fan, Y. Chen, Y. Liu, and Y. Pei, "Effect of injection strategy optimization on PCCI combustion and emissions under engine speed extension in a heavy-duty diesel engine," *Fuel*, vol. 332, p. 126053, 2023.

[23] S. Biswas, D. Kakati, P. Chakraborti, and R. Banerjee, "Performance-emission-stability mapping of CI engine in RCCI-PCCI modes under varying ethanol and CNG induced reactivity profiles: A comparative study through experimental and optimization perspectives," *Energy*, vol. 254, p. 124231, 2022.

[24] S. Natarajan, S. A. Shankar, and A. U. M. Sundareswaran, "Early Injected PCCI Engine Fuelled with Bio Ethanol and Diesel Blends - An Experimental Investigation," *Energy Procedia*, vol. 105, pp. 358–366,2017.

[25] S. Kook, S. Park, and C. Bae, "Influence of early fuel injection timings on premixing and combustion in a diesel engine," *Energy and Fuels*, vol. 22, no. 1, pp. 331–337, 2008.

[26] T. Kanda, T. Hakozaki, T. Uchimoto, J. Hatano, N. Kitayama, and H. Sono, "PCCI operation with early injection of conventional diesel fuel," *SAE Technical Paper,* no. 2005-01-0378, 2005.

[27] H. M. Kim, Y. J. Kim, and K. H. Lee, "A study of the characteristics of mixture formation and combustion in a PCCI engine using an early multiple injection strategy," *Energy and Fuels*, vol. 22, no. 3, pp. 1542–1548, 2008.

[28] X. Liang, Z. Zheng, H. Zhang, Y. Wang, and H. Yu, "A review of early injection strategy in premixed combustion engines," *Applied Sciences (Switzerland)*, vol. 9, no. 18, 2019.

[29] S. H. Park, J. Cha, H. J. Kim, and C. S. Lee, "Effect of early injection strategy on spray atomization and emission reduction characteristics in bioethanol blended diesel fueled engine," *Energy*, vol. 39, no. 1, pp. 375–387, 2012.

[30] R. Stone, Introduction to Internal Combustion Engines, 3rd ed. *Red Globe Press London*, United Kingdom, 1999.

[31] J. P. Holman, Experimental Methods for Engineers, 8th ed. *McGraw-Hill Companies*, 2012.

[32] A. Dubey, R. S. Prasad, J. Kumar Singh, and A. Nayyar, "Optimization of diesel engine performance and emissions with biodiesel-diesel blends and EGR using response surface methodology (RSM)," *Clean Energy Technologies*, vol. 8, p. 100509, 2022.

[33] R. Eyjolfsson, Design and Manufacture of Pharmaceutical Tablets: Chapter One - Introduction, *Academic Press*, Boston, 2015, pp. 1–28.

[34] A. Dubey, R. S. Prasad, J. K. Singh, and A. Nayyar, "Combined effects of biodiesel − ULSD blends and EGR on performance and emissions of diesel engine using Response surface methodology (RSM)," *Energy Nexus*, vol. 7, p. 100136, 2022.

[35] C. Zhang, Z. Chen, Q. Mei, and J. Duan, "Application of particle swarm optimization combined with response surface methodology to transverse flux permanent magnet motor optimization," *IEEE Transaction on Magnetics*, vol. 53, no. 12, 2017.

[36] M. Usman, S. Nomanbhay, M. Y. Ong, M. W. Saleem, M. Irshad, Z. U. Hassan, F. Riaz, M. H. Shah, M. A. Qyyum, M. Lee, and P. L. Show, "Response surface methodology routed optimization of performance of hydroxy gas enriched diesel fuel in compression ignition engines," *Processes*, vol. 9, no. 8, pp. 1355, 2021.

[37] J. Hunicz, J. Matijošius, A. Rimkus, A. Kilikevičius, P. Kordos, and M. Mikulski, "Efficient hydrotreated vegetable oil combustion under partially premixed conditions with heavy exhaust gas recirculation," *Fuel*, vol. 268, p. 117350, 2020.

[38] A. Jain, A. P. Singh, and A. K. Agarwal, "Effect of fuel injection parameters on combustion stability and emissions of a mineral diesel fueled partially premixed charge compression ignition (PCCI) engine," *Applied Energy*, vol. 190, pp. 658–669, 2017.

[39] O. Laguitton, C. Crua, T. Cowell, M. R. Heikal, and M. R. Gold, "The effect of compression ratio on exhaust emissions from a PCCI diesel engine," *Energy Conversion and Management*, vol. 48, no. 11, pp. 2918–2924, 2007.

[40] V. Manente, B. Johansson, and P. Tunestal, "Partially premixed combustion at high load using gasoline and ethanol, a comparison with diesel," *SAE Technical Paper,* no. 2009-01-0944, 2009.

[41] B. T. Tompkins and T. J. Jacobs, "Low-temperature combustion with biodiesel: Its enabling features in improving efficiency and emissions," *Energy and Fuels*, vol. 27, no. 5, pp. 2794–2803, 2013.

[42] M. Kaiadi, B. Johansson, M. Lundgren, and J. A. Gaynor, "Experimental investigation on different injection strategies for ethanol Partially Premixed Combustion," *SAE Technical Paper,* no. 2013-01-0281, 2013.

[43] A. P. Singh, A. Jain, and A. K. Agarwal, "Fuel-injection strategy for PCCI engine fueled by mineral diesel and biodiesel blends," *Energy and Fuels*, vol. 31, no. 8, pp. 8594–8607, 2017.

[44] R. Kiplimo, E. Tomita, N. Kawahara, S. Zhou, and S. Yokobe, "Effects of injection pressure, timing and EGR on combustion and emissions characteristics of diesel PCCI engine," *SAE Technical Paper,* no. 2011-01-1769, 2011.

[45] S. Pandey, S. Bhurat, and V. Chintala, "Combustion and emissions behaviour assessment of a partially premixed charge compression ignition (PCCI) engine with diesel and fumigated ethanol," *Energy Procedia*, vol. 160, pp. 590–596, 2019.

[46] X. B. Cheng, Y. Y. Hu, F. Q. Yan, L. Chen, and S. J. Dong, "Investigation of the combustion and emission characteristics of partially premixed compression ignition in a heavy-duty diesel engine," *Proceedings of the Institution of Mechanical Engineers, Part D: Journal of Automobile Engineering*, vol. 228, no. 7, pp. 784–798, 2014.

[47] M. D. Boot, C. C. M. Luijten, L. M. T. Somers, U. Eguz, D. D. T. M. van Erp, A. Albrecht and R.S.G. Baert, "Uncooled EGR as a means of limiting wall-wetting under early direct injection conditions," *SAE Technical Paper,* no. 2009-01-0665, 2009.

[48] M. N. V. R. S. S. Sumanth and S. Murugesan, "Experimental investigation of wall wetting effect on hydrocarbon emission in internal combustion engine," *IOP Conference Series: Materials Science and Engineering*, vol. 577, no. 1, pp. 1-10, 2019.

[49] P. Das, P. M. V. Subbarao, and J. P. Subrahmanyam, "Effect of main injection timing for controlling the combustion phasing of a homogeneous charge compression ignition engine using a new dual injection strategy," *Energy Conversion and Management*, vol. 95, pp. 248–258, 2015.

[50] J. Dernotte, J. E. Dec, and C. Ji, "Investigation of the sources of combustion noise in HCCI engines," *SAE International Journal of Engines*, vol. 7, no. 2, pp. 730–761, 2014.

[51] H. M. Baek and H. M. Lee, "Experimental investigation of ringing intensity and combustion noise level from biodiesel fuel in CRDI diesel engine with various injection timings," *Journal of Advanced Marine Engineering and Technology*, vol. 46, no. 2, pp. 56–63, 2022.

[52] M. Venkatesh Prabhu and R. Karthikeyan, "Comparative studies on modelling and optimization of hydrodynamic parameters on inverse fluidized bed reactor using ANN-GA and RSM," *Alexandria Engineering Journal*, vol. 57, no. 4, pp. 3019–3032, 2018.

[53] A. J. Shahlari, C. Hocking, E. Kurtz, and J. Ghandhi, "Comparison of compression ignition engine noise metrics in low-temperature combustion regimes," *SAE International Journal of Engines*, vol. 6, no. 1, pp. 541–552, 2013.